Three-dimensional convection-driven fronts of the exothermic chlorite-tetrathionate reaction

Gábor Schuszter,[1] Gábor Pótári,[1] Dezső Horváth,[2] and Ágota Tóth[1, a)]
[1)] *Department of Physical Chemistry and Materials Science,*
University of Szeged, Aradi vértanúk tere 1., Szeged, H-6720,
Hungary
[2)] *Department of Applied and Environmental Chemistry,*
University of Szeged, Rerrich Béla tér 1., Szeged, H-6720,
Hungary

(Dated: 10 April 2015)

Horizontally propagating autocatalytic reaction fronts in fluids are often accompanied by convective motion in the presence of gravity. We experimentally and numerically investigate the stable intricate three-dimensional pattern arising in the exothermic chlorite–tetrathionate reaction as a result of the antagonistic thermal and solutal contribution to the density change. By particle image velocimetry measurements we construct the flow field that stabilizes the front structure. The calculations applied for incompressible fluids using the empirical rate-law model reproduce the experimental observations with good agreement.

[a)] E-mail: atoth@chem.u-szeged.hu

A vertical reaction front separating the reactants and products with different density gives rise to hydrodynamic instability under gravity. The propagating front becomes tilted as the less dense fluid tends to advance on top of the other. When this reactive interface is driven by an exothermic reaction, multicomponent convection can evolve due to the interplay of thermal and solutal contributions to the density change. In a three-dimensional medium, the resultant complex flow pattern can sustain a stable intricate front structure propagating at a constant velocity. The flow field determined experimentally by using particle image velocimetry reveals that the single large convection roll rotating at the tip of the front creates the smooth leading edge and transforms into a pair of counter-rotating vortices that stabilize the center cusp at the tail of the reaction front. Numerical solution of the Navier-Stokes equation using the empirical rate-law of the reaction can successfully reconstruct the characteristics of the experimental flow field.

I. INTRODUCTION

Self-organized chemical structures arise from the coupling between a chemical reaction with positive feedback and a transport process.[1] The resultant spatial patterns are characterized by the underlying concentration distribution significantly different from that of the uniform steady-state. Most often research, both theoretical and experimental, has focused on thin layers allowing convenient monitoring of the reaction and representing a two-dimensional medium. The first systematic studies of pattern formation in a three-dimensional medium have appeared in reaction-diffusion systems of excitable reactions, where the various dynamics of the filaments in scroll waves represent behavior absent in two dimensions[2–4], followed by studies of Turing patterns.[5,6] The introduction of the third dimension makes a difference even in the behavior of the simplest chemical pattern, a propagating reaction front defined by the narrow zone spatially separating the reactant and the autocatalytic product: a critical radius for local initiation exists for cubic autocatalysis only in three dimensions.[7]

In a chemical reaction partial molar volumes vary because of the change in chemical composition, giving rise to a change in the density of the solution, which can also result from local temperature rise or fall due to the exo- or endothermicity of the reaction, respectively. Under normal gravity a small density change of 0.1 kg/m^3 in liquids can generate fluid flow that can have significant contribution to pattern formation.[8] When the solutal and thermal components of the density change act cooperatively, generally simple convection occurs, whereas their antagonistic behavior can lead to multicomponent convection.[9] When thermal effects come into play in thicker solution layers with insufficient heat removal, multicomponent convection arises in the chlorite–tetrathionate (CT) front, since the reaction is exothermic leading to a local increase in temperature at the front.[10–12] Thermal contribution in the iodate–arsenous acid (IAA) reaction is less dramatic, since the enthalpy of reaction is significantly smaller and the liberated heat acts cooperatively to the solutal component of the density change.[13,14] These two prototype reaction fronts have been studied in great details both experimentally[15–17] and theoretically[18–25] in thin layers.

Less is known about the convective instabilities in association with autocatalytic fronts in three-dimensional media where thermal effects are inevitable, resulting in complicate patterns.[10,26] In the IAA reaction a switch between the reactive states has been observed in a three-dimensional medium.[27] In a cylindrical column the same reaction produces symmetric ascending plumes as a result of the cooperative solutal and thermal contributions to density change.[28–30] When these two components compete in the CT reaction, both oscillatory and stationary traveling three-dimensional patterns can arise on the millimeter scale around the inversion of the density change.[31] In the CT reaction when thermal effects dominate, resulting in a density decrease at the reaction front, widening the reaction medium can stabilize the horizontally propagating front.[32] The resultant self-sustained tilted structure reveals a very intricate pattern having a smooth leading edge and a sharp center cusp at the tail. Surprisingly however both its shape and velocity of propagation are constant in time.

In this work our aim is to thoroughly investigate the flow pattern underlying this complex front structure propagating horizontally. We utilize particle image velocimetry (PIV) and setup both vertical and horizontal light sheets at various locations to reconstruct the entire three-dimensional flow field. We also carry out a modeling study based on the empirical rate-law of the reaction and calculate the flow field in accordance with the experimental parameters.

II. MODELING STUDY

The governing equations for the chlorite–tetrathionate reaction according to

$$2S_4O_6^{2-} + 7ClO_2^- + 6H_2O \longrightarrow 8SO_4^{2-} + 7Cl^- + 12H^+ \tag{1}$$

in slight excess are based on the empirical rate law of Eq. (1) as

$$R = k[S_4O_6^{2-}]\left([ClO_2^-]_0 - \frac{7}{2}[S_4O_6^{2-}]_0 + \frac{7}{2}[S_4O_6^{2-}]\right)[H^+]^2 \ , \tag{2}$$

where R is the rate of reaction for unit volume, while $[ClO_2^-]_0$ and $[S_4O_6^{2-}]_0$ are the initial concentrations of reactants far ahead of the reaction front. In Eq. (2) we take advantage of the stoichiometry of the reaction, which allows the elimination of the component balance for chlorite ion. Hence the reaction–diffusion–convection system describing the propagating reaction front is governed by

$$\frac{\partial[S_4O_6^{2-}]}{\partial t} + \vec{u}\cdot\nabla[S_4O_6^{2-}] = D\nabla^2[S_4O_6^{2-}] - 2R \ , \tag{3a}$$

$$\frac{\partial[H^+]}{\partial t} + \vec{u}\cdot\nabla[H^+] = D_{H^+}\nabla^2[H^+] + 12R \ , \tag{3b}$$

$$\frac{\partial T}{\partial t} + \vec{u}\cdot\nabla T = \frac{\lambda}{\rho c_p}\nabla^2 T - \frac{\Delta_r H}{\rho c_p}R \ , \tag{3c}$$

$$\frac{\partial \vec{u}}{\partial t} + \vec{u}\cdot\nabla\vec{u} = \nu\nabla^2\vec{u} - \frac{\nabla p}{\rho_0} + \frac{\rho}{\rho_0}\vec{g} \ , \tag{3d}$$

which comprises the differential component balance equation for tetrathionate and hydrogen ion, the differential energy balance equation, and the Navier-Stokes equation representing the conservation of linear momentum. In Eq. (3a) D is the diffusion coefficient of the reactants, while in Eq. (3c) λ and c_p are the thermal conductivity and the specific heat capacity of the solution respectively, and $\Delta_r H$ symbolizes the enthalpy of reaction. In Eq. (3d) ν and ρ are the kinematic viscosity and the density of the solution, while ρ_0 is the density of water. In the experimental system the liquid may be considered incompressible, i.e, $\nabla\cdot\vec{u} = 0$, therefore the density changes are neglected except in the buoyancy term, which corresponds to the Boussinesq approximation. The density of solution is considered to be a linear function of both the concentration of the limiting reactant ($[S_4O_6^{2-}]$) and temperature (T), hence $\rho = \rho_0 + \rho_C[S_4O_6^{2-}] + \rho_T(T - T_0)$, where T_0 is the initial temperature of the reactant solution.

We keep the differential equations in Eq. (3) in dimensional form and select physically acceptable parameters without fitting. For the diffusion coefficient of the reactants we take

$D = 2 \times 10^{-9}$ m^2/s, a value associated with small hydrated ions, while for the autocatalyst $D_{\mathrm{H}^+} = 4 \times 10^{-9}$ m^2/s, which reflects the greater diffusivity of hydrogen ion in aqueous solutions.[33] The initial concentration of tetrathionate ion is equal to the experimental value of $[\mathrm{S_4O_6^{2-}}]_0 = 5.0$ mmol/L. The enthalpy of reaction $\Delta_r H = -3960$ kJ/mol is known from calorimetric measurements, and the solutal component of density change with respect to the reactant concentration $\rho_C = -0.05$ kg/mol is obtained from density measurements. It is important to point out that the sign of ρ_C arises from relating the solution density to the limiting reactant tetrathionate. Its concentration decreases in the course of the reaction, while the density increases as a result of the compositional change as mentioned in the introduction. Under the experimental conditions both the reactant and the product mixtures are regarded as dilute solutions, therefore for the rest of the physical parameters the appropriate values for water are taken as $\nu = 10^{-6}$ m^2/s, $\rho_0 = 10^3$ kg/m^3, $\rho_T = -0.284$ kg/(K m^3), $\lambda = 0.61$ (kg m)/(K s^3), and $c_p = 4186$ J/(K kg)[16,34,35].

The boundary conditions for the closed system are defined as zero-gradients for the concentrations and temperature, the latter condition is equivalent to insulating walls. A fix value of (0,0,0) for the fluid velocity ($\vec{u}$) represents no-slip walls, while for pressure the $\vec{n} \cdot \nabla p = -(\vec{n} \cdot \nabla \rho)(\vec{g} \cdot \vec{r})$ expression, i.e., buoyant pressure is used.

The differential equations of Eq. (3) are solved on a rectangular, three-dimensional grid of 400 × 45 × 60 block elements, corresponding to a physical size of 200 mm × 20 mm × 10 mm, by finite volume method. For the calculations the OpenFOAM package[36] is used with the code running in parallel mode using the openMPI implementation of Message Passing Interface (MPI). The Navier-Stokes equation in Eq. (3d) is solved by applying the pressure implicitly with splitting of operators (PISO) algorithm for corrected velocity and pressure values.[37] The time derivatives are expressed with implicit Euler method with time steps taken to be 10^{-3} s. The gradients are approximated by Gauss linear, the divergence with Gauss upwind and the Laplace operator with Gauss linear uncorrected methods. The obtained algebraic equations are then solved by a preconditioned biconjugate gradient method, where the preconditioning matrix is constructed by the diagonal incomplete lower–upper method with an absolute error of 10^{-12} for velocity, pressure, and concentrations.

III. EXPERIMENTAL

The experiments are carried out with purchased chemicals (Sigma-Aldrich) without any further purification. The solution with composition $[K_2S_4O_6] = 5$ mmol/L, $[NaClO_2] = 20$ mmol/L, $[NaOH] = 5$ mmol/L, and $[\mathrm{bromophenolblue}] = 4.8 \times 10^{-3}$ mmol/L are mixed at room temperature. Light scattering particles (latex beads, 6.4 μm in diameter, Sigma-Aldrich) are then added in 0.01 mass ratio. The reactant solution is immediately injected into the reaction vessel with an automatic pipette; the scheme of the experimental setup is shown in Fig. 1. The light of a laser source (Roithner LaserTechnik with 532 nm wavelength, 100 mW electric power) is expanded into a sheet containing parallel beams with two convex lenses (Techspec). The reaction vessel is placed on a movable table which can be positioned with 0.01 mm precision, allowing the variation of the location and orientation of the light sheets.

To initiate a vertical reaction front, the autocatalyst hydrogen ion is electrochemically generated by using a pair of U-shaped platinum electrodes and applying 3 V potential difference between them for 5 s. The reaction front is monitored from a direction transverse to the direction of propagation by a black and white or color CCD camera. An imaging system is used to capture the images with 0.2 s time intervals, which are later processed using in-house software. We have repeated the experiments with vertical light sheets in 10 different y-positions and horizontal light sheets with 4 different z-positions (front propagation is along the x-axis). Over all, more than 100 experiments have been carried out to ensure the reproducibility and comparability of the cross sections in every places.

The captured images with 1024 pix × 768 pix size are split into 64 pix × 64 pix interrogation windows, and the vector of average displacement corresponding to each window is determined by calculating the spatial correlation between two gray scale functions related to the successive images.[38,39] The spatial correlation is calculated using the Fourier-transforms according to

$$C(f, g) \equiv f(m, n) \circ g(m, n) \Leftrightarrow F(\xi, \eta) G^{\star}(\xi, \eta) \ , \tag{4}$$

where functions f and g represent the digitized images in time t and $t + dt$, F is the Fourier-transform of f and $G^{\star}$ is the complex conjugate of the Fourier-transform of g. The displacement vector assigned to the interrogation window corresponds to the location of maximum of the correlation function. In order to achieve the required spatial resolution, the field view in the direction of propagation is set to be less then 13 mm, therefore five images with appropriate time delay between them is necessary to fit the entire reaction front into a single image. The time delay is determined from the velocity of front propagation. The images containing the light scattered from vertical sheets provide the u_x and u_z components of the velocity field ($\vec{u}$) at preset y-coordinates, while those from horizontal light sheets the u_x and u_y components. The common u_x values allow the reconstruction of the entire velocity field by matching the appropriate coordinates.

IV. RESULTS & DISCUSSION

The vertical reaction front initiated by the electrolysis soon becomes tilted as a result of the fluid motion brought about by buoyancy effects. The reaction container creates a three-dimensional domain where the physical extent of the system does not allow sufficient heat removal, therefore temperature rises in bulk of the solution. The thermal contribution to the density change supersedes the solutal component at these concentrations, hence the product formed at the thin reaction front is less dense than the reactant far ahead, hence the solution advances ahead on the top. Following a short transient time, a complex but stationary front structure evolves that propagates at a constant velocity in accordance with earlier experimental studies. The front has a smooth leading edge forming a single cell in the vertical projection of the image and ends in a sharp center cusp that is visible in both the vertical and the horizontal projection (see Fig. 2).

The flow field behind this intricate front structure is presented in Fig. 3(a). Color coding of the arrows is used for indicating the strength of the flow: the order red–yellow–green–blue corresponds to decreasing velocity. Four vertical cuts normal to the front propagation, i.e. in the (y, z)-plane, at selected x-coordinates are shown separately in order to better illustrate the dynamics of the flow. The leading tip of the reaction front is characterized with a more less uniform downward flow apparent in Fig. 3(e). The return flow of this system-wide convection roll breaks up, significant upward flow only occurs at $y = 7$ mm and at $y = 13$ mm, as shown in Fig. 3(d). The location of these two zones with ascending solution corresponds to that of the two thin blue stripes parallel to the direction of front propagation, visible in the projection shown in Fig. 2(a), indicating that the return flow brings fresh reactant solution into the reaction front. Moving back in the reaction front, the upward flow weakens while the downward flow strengthens, especially in the centerline (see Fig. 3(c)). Figure 3(b) however reveals that two symmetric vortices counter-rotating in the (y, z)-plane reverse the flow in the center of the container. This ascending solution centered at $y = 10$ mm is responsible for the appearance of the trailing cusp seen in Fig. 2(b). No significant fluid motions is observed beyond this region, the entire container is filled with the acidic product mixture as the limiting tetrathionate reactant has been all consumed.

In the solution of Eq. (3), the calculated reaction front also takes on a stable profile and travels at a constant velocity of 1.03 mm/s in agreement with the experimentally measured 1.06 ± 0.01 mm/s. In accordance with the experimental observations, the front has a complicated structure as shown in Fig. 4. As it advances in the top layer, it forms a single cell presented in Fig. 4(a), while the front breaks up into the three cells in the lower layer (see Fig. 4(b)). The false coloring used in the figure tries to mimic the experimental scenario, dark blue color indicates the reactant mixture and light yellow the product. Upon constructing the vertical projection of the front image, corresponding to the experimental view in Fig. 2(a), not only the smooth leading edge but also the two blue lines behind it are reproduced by the calculations. The lack of the V-shaped trail cusp, visible if Fig. 2(b), is attributed to the failure of the simple empirical rate law model at greater reaction coordinates[40,41] and to the improper rendering of the color change of the pH-indicator by the false coloring applied for mapping the concentration field, but the underlying fluid motion—as we shall see—will match that observed experimentally. The calculated temperature rise (3 K) in the course of the reaction is also in good agreement with the experimental measurements of our earlier study.

We present the calculated velocity field in the same fashion as that determined by the PIV measurements. As the warmer and less dense product advances on the top, it forces the reactant to move downward (see Fig. 5(a,e)) and creates a wide convection roll and a smooth leading edge. The return flow behind it, shown in Fig. 5(d), breaks the reaction front into three cells, since strong upward flow only appears $y = 7$ mm and at $y = 13$ mm, similarly to the experiments. The locally ascending fresh reactant is also responsible here for the visible blue lines behind the leading edge. Further back, the downward flow strengthens as the outer convection rolls grow in size, presented in Fig. 5(c). The calculated flow is also reversed along the centerline when the two counter-rotating vortices in Fig. 5(b) come into contact forming the back of the front in accordance with the experimental behavior.

Tracing the axis line of the main vortex reveals that the axis, originally oriented transverse to the direction of propagation, curls at the sides as shown in Fig. 6. This is the result of the imperfect insulation at the walls, which leads to lower temperature and hence greater density compared to the bulk of the liquid, generating a downward fluid flow. A pair of minor vortex also evolves behind the tip which shifts downward. The center flow reverses its direction when these two, indicated with dashed lines Fig. 6, diminish, leaving the remnant of the original convection roll behind.

V. CONCLUSIONS

Our experimental study of the flow field behind the intricate front structure reveals that the single large convection roll allowing the warmer product to advance on the top is transformed into a pair of counterrotating vortices by the side walls. The driving force is the imperfect insulation of the system that inevitably arises in a three-dimensional medium: the liquid at the boundary becomes colder than the inner region for an exothermic reaction. When the system is sufficiently wide, the boundary conditions allow the generation of stable convection rolls leading to stationary structures. The work also emphasizes that thermal effects in a three-dimensional medium cannot be neglected in most cases, even if they have stabilizing contribution.

ACKNOWLEDGMENTS

The authors dedicate this paper to Professor Irv Epstein on celebration of his 70th birthday for his outstanding contribution to nonlinear science. This work was financially supported by the European Space Agency (ESTEC 4000102255/11/NL/KML). The authors are grateful to the Hungarian Supercomputer Center, NIIF, and HPC Szeged for the computational facility. G. Pótári gratefully acknowledges the support by the National Excellence Program (TÁMOP 4.2.4.A/2-11-1-2012-0001).

REFERENCES

[1] I. R. Epstein and J. A. Pojman, *An Introduction to Nonlinear Dynamics: Oscillations, Waves, Patterns, and Chaos* (Oxford University Press, Oxford, 1998)

[2] T. Bánsági Jr. and O. Steinbock, "Nucleation and collapse of scroll rings in excitable media," Phys. Rev. Lett. **97**, 198301 (2006)

[3] T. Bánsági Jr. and O. Steinbock, "Three-dimensional spiral waves in an excitable reaction system: Initiation and dynamics of scroll rings and scroll ring pairs," Chaos **18**, 026102 (2008)

[4] D. Kupitz and M. J. B. Hauser, "Helical deformation of the filament of a scroll wave," Phys. Rev. E **86**, 066208 (2012)

[5] T. Bánsági Jr., V. K. Vanag, and I. R. Epstein, "Tomography of reaction-diffusion microemulsion reveals three-dimensional turing patterns," Science **331**, 1309–1312 (2011)

[6] T. Bánsági Jr., V. K. Vanag, and I. R. Epstein, "Two- and three-dimensional standing waves in a reaction-diffusion system," Phys. Rev. E **86**, 045202 (2012)

[7] D. J. Needham and J. H. Merkin, "The effect of geometrical spreading in two and three dimensions on the formation of travelling wavefronts in a simple, isothermal, chemical system," Nonlinearity **5**, 413–452 (1992)

[8] I. Nagypál, G. Bazsa, and I. R. Epstein, "Gravity-induced anisotropies in chemical waves," J. Am. Chem. Soc. **108**, 3635–3640 (1986)

[9] J. A. Pojman and I. R. Epstein, "Convective effects on chemical waves. 1. mechanism and stability criteria," J. Phys. Chem. **94**, 4966–4972 (1990)

[10] L. Rongy, G. Schuszter, Z. Sinkó, T. Tóth, D. Horváth, Á. Tóth, and A. De Wit, "Influence of thermal effects on buoyancy-driven convection around autocatalytic chemical fronts propagating horizontally," Chaos **19**, 023110 (2009)

[11] L. Rongy and A. De Wit, "Buoyancy-driven convection around exothermic autocatalytic chemical fronts traveling horizontally in covered thin solution layers," J. Chem. Phys. **131**, 184701 (2009)

[12] P. Grosfils, F. Dubois, C. Yourassowsky, and A. De Wit, "Hot spots by simultaneous experimental measurement of the two-dimensional concentration and temperature fields of an exothermic chemical front during finger-pattern formation," Phys. Rev. E **79**, 017301 (2009)

[13] L. Šebestíková, J. D'Hernoncourt, M. J. B. Hauser, S. C. Müller, and A. De Wit, "Flow-field development during finger splitting at an exothermic chemical reaction," Phys. Rev. E **75**, 026309 (2007)

[14] J. Martin, N. Rakotomalala, L. Talon, and D. Salin, "Measurement of the temperature profile of an exothermic autocatalytic reaction front," Phys. Rev. E **80**, 055101 (2009)

[15] M. Böckmann and S. C. Müller, "Growth rates of the buoyancy-driven instability of an autocatalytic reaction front in a narrow cell," Phys. Rev. Lett. **85**, 2506–2509 (2000)

[16] D. Horváth, T. Bánsági Jr., and Á. Tóth, "Orientation-dependent density fingering in an acidity front," J. Chem. Phys. **117**, 4399–4401 (2002)

[17] T. Bánsági Jr., D. Horváth, and Á. Tóth, "Convective instability of an acidity front in Hele-Shaw cells," Phys. Rev. E **68**, 026303 (2003)

[18] J. Huang, D. A. Vasquez, B. F. Edwards, and P. Kolodner, "Onset of convection for autocatalytic reaction fronts in a vertical slab," Phys. Rev. E **48**, 4378–4386 (1993)

[19] D. A. Vasquez, J. M. Littley, J. W. Wilder, and B. F. Edwards, "Convection in chemical waves," Phys. Rev. E **50**, 280–284 (1994)

[20] D. A. Vasquez, J. W. Wilder, and B. F. Edwards, "Chemical wave propagation in Hele-Shaw cells and porous media," J. Chem. Phys. **104**, 9926–9931 (1996)

[21] A. De Wit, "Fingering of chemical fronts in porous media," Phys. Rev. Lett. **87**, 054502 (2001)

[22] J. Martin, N. Rakotomalala, D. Salin, and M. Böckmann, "Buoyancy-driven instability of an autocatalytic reaction front in a Hele-Shaw cell," Phys. Rev. E **65**, 051605 (2002)

[23] A. De Wit, "Miscible density fingering of chemical fronts in porous media or Hele-Shaw cells: nonlinear simulations," Phys. Fluids **16**, 163 (2004)

[24] S. Kalliadasis, J. Yang, and A. De Wit, "Fingering instabilities of exothermic reaction-diffusion fronts in porous media," Phys. Fluid **16**, 1395 (2004)

[25] L. Rongy, N. Goyal, E. Meiburg, and A. De Wit, "Buoyancy-driven convection around chemical fronts traveling in covered horizontal solution layers," J. Chem. Phys. **127**, 114710 (2007)

[26] T. Tóth, D. Horváth, and Á. Tóth, "Thermal effects in the density fingering of the chlorite-tetrathionate reaction," Chem. Phys. Lett. **442**, 289–292 (2007)

[27] L. Šebestíková and M. J. B. Hauser, "Buoyancy-driven convection may switch between reactive states in three-dimensional chemical waves," Phys. Rev. E **85**, 036303 (2012)

[28] M. C. Rogers and S. W. Morris, "Buoyant plumes and vortex rings in an autocatalytic chemical reaction," Phys. Rev. Lett. **95**, 024505 (2005)

[29] M. C. Rogers, M. D. Mantle, A. J. Sederman, and S. W. Morris, "Conduits of steady-state autocatalytic plumes," Phys. Rev. E **77**, 026105 (2008)

[30] M. C. Rogers and S. W. Morris, "The heads and tails of buoyant autocatalytic balls," Chaos **22**, 037110 (2012)

[31] O. Miholics, T. Rica, D. Horváth, and Á. Tóth, "Oscillatory and stationary convective patterns in a reaction driven gravity current," J. Chem. Phys. **135**, 204501 (2011)

[32] É. Pópity-Tóth, D. Horváth, and Á. Tóth, "Horizontally propagating three-dimensional chemo-hydrodynamic patterns in the chlorite-tetrathionate reaction," Chaos **22**, 037105 (2012)

[33] É. Pópity-Tóth, G. Pótári, I. Erdős, D. Horváth, and Á. Tóth, "Marangoni instability in the iodate-arsenous acid reaction front," J. Chem. Phys. **141**, 044719 (2014)

[34] M. L. V. Ramires, C. A. N. de Castro, Y. Nagasaka, A. Nagashima, M. J. Assael, and W. A. Wakeham, "Standard reference data for the thermal conductivity of water," J. Phys. Chem. Ref. Data **24**, 1377–1381 (1995)

[35] R. C. Weast, ed., *Handbook of Chemistry and Physics* (CRC Press Inc., Cleveland, 1974)

[36] H. G. Weller, G. Tabor, H. Jasak, and C. Fureby, "A tensorial approach to computational continuum mechanics using object orientated techniques," Computers in Physics **12**, 620–631 (1998)

[37] R. I. Issa, "Solution of the implicitly discretised fluid flow equations by operator-splitting," J. Comp. Phys. **62**, 40–65 (1985)

[38] S. P. McKenna and W. R. McGillis, "Performance of digital image velocimetry processing techniques," Experiments in Fluids **32**, 106–115 (2002)

[39] M. Raffel, C. E. Willert, S. T. Wereley, and J. Kompenhans, *Particle Image Velocimetry: A Practicle Guide* (Springer, Berlin, 2007)

[40] A. K. Horváth, "A three-variable model for the explanation of the supercatalytic effect of hydrogen ion in the chlorite-tetrathionate reaction," J. Phys. Chem. A **109**, 5124–5128 (2005)

[41] A. K. Horváth, I. Nagypál, and I. R. Epstein, "Three autocatalysts and self-inhibition in a single reaction: A detailed mechanism of the chlorite-tetrathionate reaction," Inorg. Chem. **45**, 9877–9883 (2006)

Fig. 1 The sketch of the experimental setup showing the vertically oriented laser sheet.

Fig. 2 Top view (a) and side view (b) of the chlorite–tetrathionate reaction front with stationary shape observed experimentally in the three-dimensional domain. Dark blue color corresponds to the reactant and light yellow color to the product solution. The field of view is 10 cm × 2 cm (a) and 10 cm × 1 cm (b).

Fig. 3 Flow field determined experimentally in the three-dimensional reaction medium (a) and the cross sections at different distances from the tip of the front profile (b, c, d, e). Colors from red to blue correspond to the flow velocity from high to low. Dashed red arrows are drawn to guide the eye to the main flow directions.

Fig. 4 Cross sections of the calculated concentration field at $z = 9$ mm (a) and $z = 5$ mm (b). Also shown is the concentration averaged along z-axis (c) to correspond to Fig. 2(a). False coloring mimics the behavior of the pH indicator used in the experiments: dark blue color represents the reactant and light yellow the product solution. The field of view is 9.5 cm × 2 cm.

Fig. 5 Concentration averaged along the y-axis (a) to correspond to Fig. 2(b). Coloring is the same as in Fig. 4. Also shown are the cross sections with the calculated flow field at different distances from the tip of the front profile (b, c, d, e) similarly to Fig. 3 with $x = 0$ indicating the mean front position. Dashed red arrows are drawn to guide the eye to the main flow directions.

Fig. 6 Axis line of the dominating vortex that maintaines the stable reaction front, obtained by tracing the maximum of $|\nabla \times \vec{u}|$. Dotted line follows the axis of minor vortices that contribute in shaping the spatiotemporal structure. Also shown are the positions of the vertical cross sections in Figs. 5(b-e).

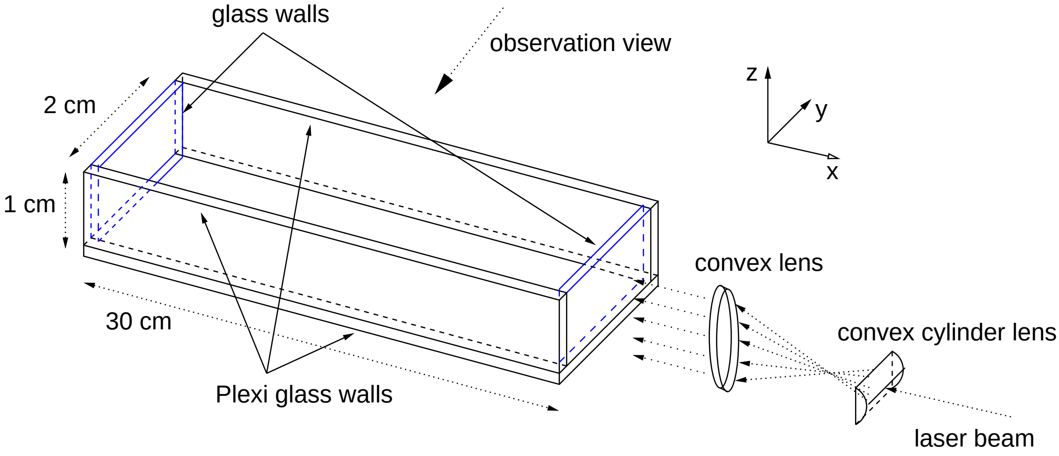

FIG. 1. G. Schuszter ... Chaos

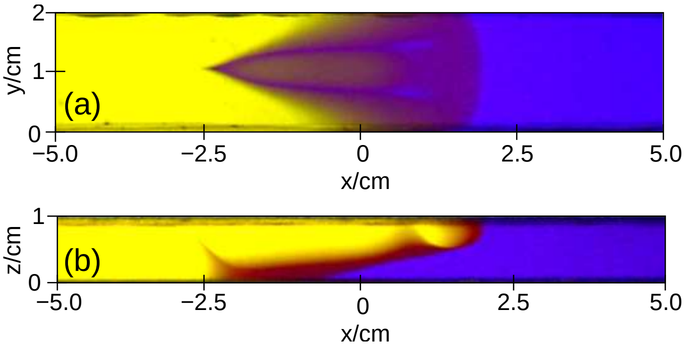

FIG. 2. G. Schuszter ... Chaos

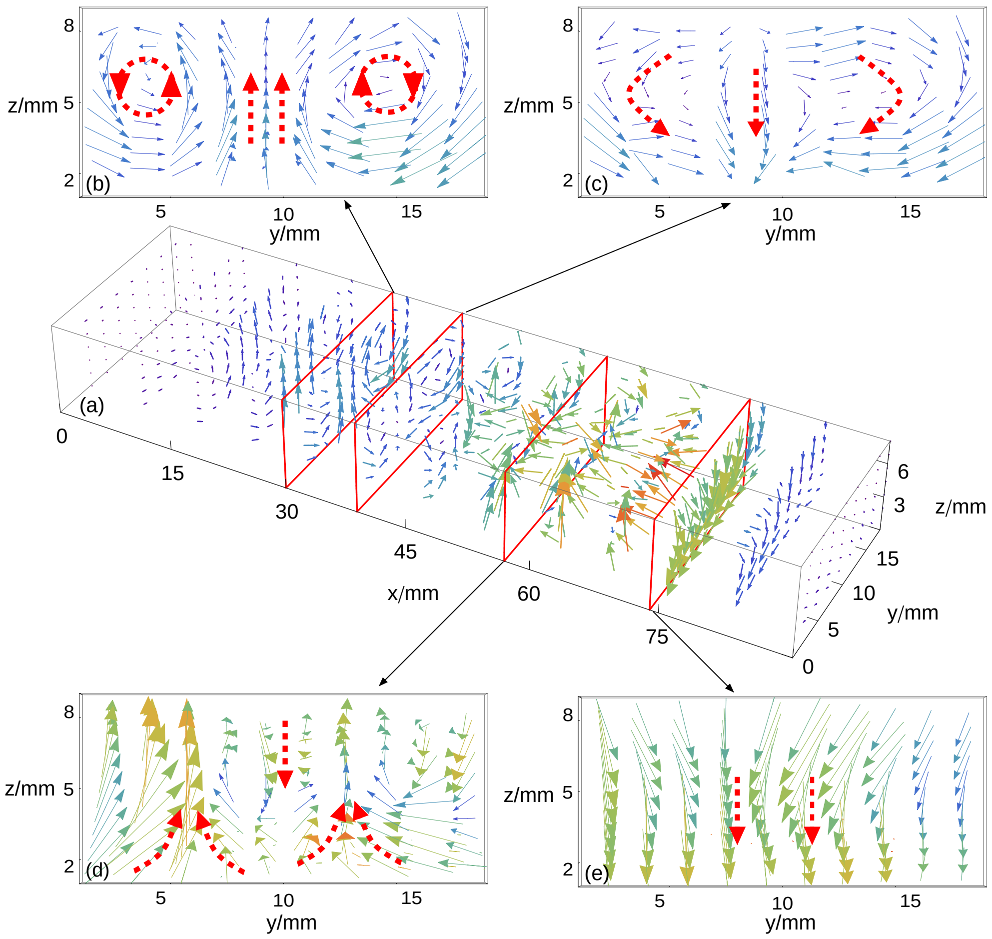

FIG. 3. G. Schuszter ... Chaos

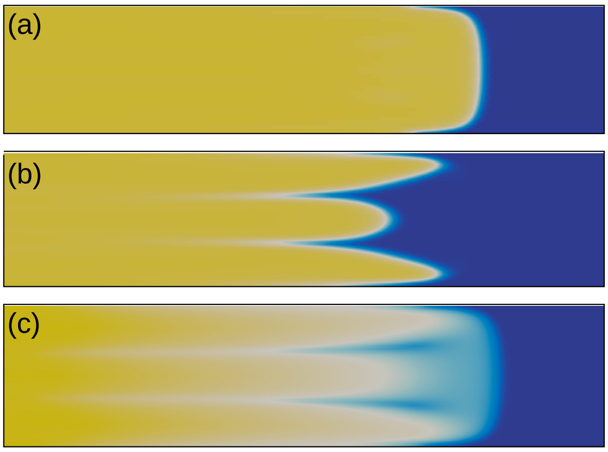

FIG. 4. G. Schuszter ... Chaos

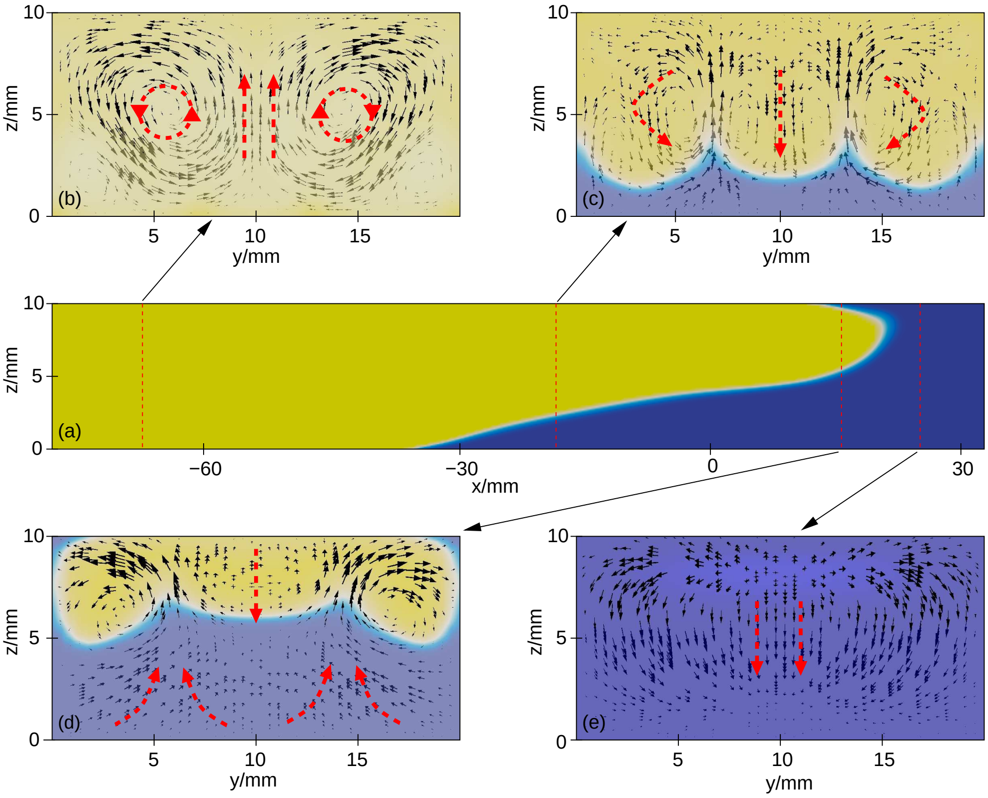

FIG. 5. G. Schuszter ... Chaos

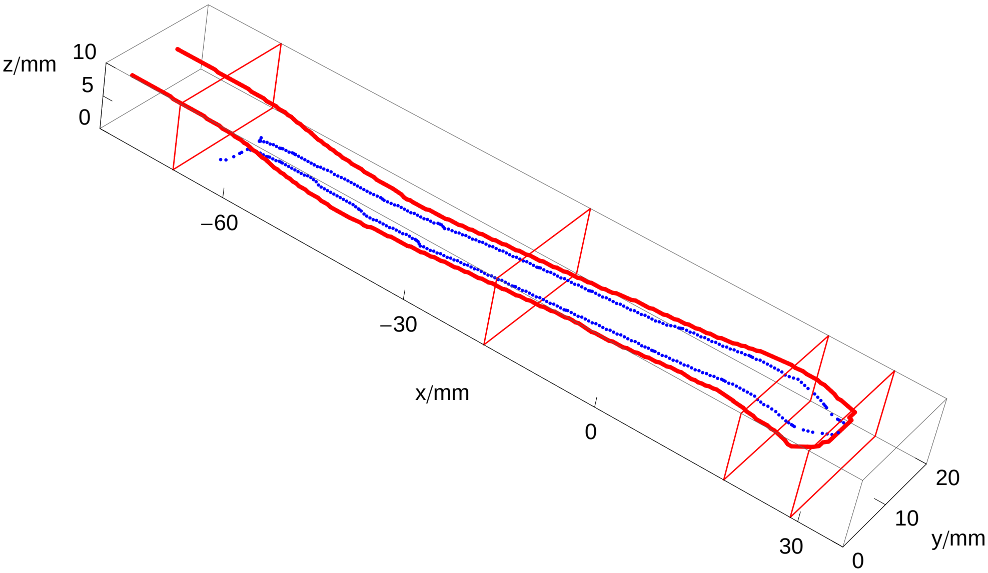

FIG. 6. G. Schuszter ... Chaos